

DRAFT VERSION JANUARY 30, 2026
 Typeset using **LATEX** **preprint** style in AASTeX631

Balancing Variety and Sample Size: Optimal Parameter Sampling for Ariel Target Selection

EMILIE PANEK ,¹ ALEXANDER ROMAN ,¹ KATIA MATCHEVA ,¹ KONSTANTIN T. MATCHEV ,¹ AND NICOLAS B. COWAN ,^{2,3}

¹*Department of Physics and Astronomy, University of Alabama, Tuscaloosa, AL, 35487, USA*

²*Department of Earth & Planetary Sciences, McGill University, 3450 University St, Montréal, H3A 2A7, Canada*

³*Department of Physics, McGill University, 3600 University St, Montréal, QC H3A 2T8, Canada*

Submitted to ApJ

ABSTRACT

Targeted astrophysical surveys are limited by the amount of telescope time available, which makes it impossible to observe every single object of interest. In order to maximize the scientific return, we need a well thought strategy for selecting the observational targets, in our case exoplanets. This study evaluates various strategies for selecting exoplanet targets within limited observation windows, focusing specifically on the selection of exoplanet targets for Tier 2 transit spectroscopy with ESA’s upcoming Ariel mission. We define three distinct selection criteria—sample size, variance, and leverage—and translate them into objective functions compatible with modern optimization algorithms. Specifically, we test five heuristics for maximizing sample leverage: leverage greedy, simulated annealing, K-means clustering, regular classes, and quantile classes. The performance of these methods is demonstrated through three practical exercises across one, two, and three parameters of diversity. Each criterion represents a unique trade-off between sample size, diversity, and total observation time. While a time-greedy approach maximizes the quantity of planets, it fails to capture diversity. Conversely, variance-greedy selection prioritizes diversity but introduces significant drawbacks: it oversamples rare cases and undersamples typical planets, ultimately reducing the total number of targets observed. Leverage-based selections emerge as the most effective middle ground, successfully balancing sample diversity with a robust sample size. This work supports the broader community effort to ensure that Ariel delivers the most diverse and scientifically valuable sample of exoplanet atmospheres within mission limits.

Keywords: Exoplanets (498) — Exoplanet astronomy (486) — Sampling Distribution (1899) — Transmission spectroscopy (2133)

Corresponding author: Emilie Panek
 epanek1@ua.edu

1. INTRODUCTION

The Ariel mission (Atmospheric Remote-sensing Infrared Exoplanet Large-survey) is a space telescope led by ESA, planned to launch in 2029 (Tinetti et al. 2018; Tinetti et al. 2021). It will operate in synergy with ongoing and planned missions such as JWST (Gardner et al. 2006, 2023), Twinkle (Edwards et al. 2019; Stosbury et al. 2022; Zhang et al. 2025), Pandora (Barclay et al. 2025) and Plato (Rauer et al. 2025). Ariel is uniquely designed for population-level studies of exoplanet atmospheres rather than single-object characterization. It aims to obtain spectral information for close to 1000 transiting exoplanets, which would allow to build a significant understanding of the physics and chemistry of a wide range of exoplanets. However, with more than 6000 confirmed transiting exoplanets (see <https://exoplanetarchive.ipac.caltech.edu/> for the up-to-date number of confirmed exoplanets) one is forced to make certain selection choices to maximize the science return of the telescope within its 4-year primary mission. The problem of optimal target selection for Ariel and similar missions has received increasing attention in recent literature. It has been realized that selecting a subsample optimized for individual atmospheric studies does not guarantee the best constraints on the global population parameters (Batalha et al. 2023). Cowan & Coull-Neveu (2025) pointed out that the precision with which we can quantify population trends is determined by the number of targets N in the survey and their variance V . The authors introduced the notion of leverage, namely $L = \sqrt{NV}$, as a compromise between the multiplicity and diversity of the observed planets. This choice was motivated by the fact that the uncertainty on the inferred slope of a linear trend is inversely proportional to the leverage. Subsequent work in Burt et al. (2025) emphasized the importance of sampling more evenly across a range of planet radii and equilibrium temperatures. It also considered the additional costs in terms of ground-based telescope time to reduce the uncertainties in the orbital planet parameters.

The specific problem considered here — optimal target selection subject to a finite observational budget — falls into a general class of problems in optimization theory known as submodular maximization with a knapsack constraint. Submodular maximization implies a property of diminishing returns, where adding an element to a small subset helps more than adding it to a large subset. A knapsack constraint means that each selected element i comes with a cost (in this case this is the required observational time t_i by Ariel) and that there exists an overall budget which should not be exceeded (in our case, the total lifetime T of the Ariel mission). Thus we can write the constraint as

$$\sum_{i=1}^N t_i \leq T, \quad (1)$$

where $N = |\mathcal{S}|$ is the number of elements in the selected subsample \mathcal{S} of observational targets.

A key step is the choice of an objective function $f(\mathcal{S})$ that reflects the scientific merit of the selected subsample $\mathcal{S} \subseteq \mathcal{T}$, where \mathcal{T} spans the entire available set of options. To be specific, in this paper we focus on the Ariel Mission Candidate Sample (hereafter referred as MCS) list (Edwards & Tinetti 2022), that defines the entire set \mathcal{T} which we can choose from. Following Cowan & Coull-Neveu (2025), in this paper we shall primarily adopt the leverage as our objective function, but for illustration we shall also consider alternative choices for f , since different choices of f would result in different optimal selection outcomes for \mathcal{S} .

After settling on an objective function f , it is still necessary to pick the set of planetary parameters $\{p\}$ that will be used as axes of diversity. Common choices include the planetary radius R_p , the

planet equilibrium temperature T_p , and sometimes the stellar effective temperature T_s (Edwards & Tinetti 2022; Batalha et al. 2023; Hord et al. 2024; Cowan & Coull-Neveu 2025; Burt et al. 2025). In our study we shall consider those three parameters as well, i.e., $\{p\} = \{R_p, T_p, T_s\}$.

The resulting numerical task of selecting a subset \mathcal{S} which maximizes the objective function $f(\{p\})$ subject to the budgetary constraint (1), is in general far from trivial. A brute force approach (considering all possible candidate selections \mathcal{S}) is impossible since in the case of Ariel, this is an astronomical number of combinations, on the order of 10^{650} (Cowan & Coull-Neveu 2025). This is why one tends to rely on simple heuristics or figures-of-merit for each planet in order to arrive at an approximate solution. For example, Cowan & Coull-Neveu (2025) developed a class-based approach, by binning along each parameter axis, thus dividing the set \mathcal{T} into different categories (thus aiming for diversity) and then cyclically choosing the easiest to observe planet in each category. While sensible, this heuristic does not guarantee that the selected subsample \mathcal{S} is globally optimal. In this paper we propose a greedy algorithm which directly targets the optimization of the objective function f and yields a globally optimal selection for \mathcal{S} . We compare our method to the previous approaches in the literature and demonstrate that it gives a superior selection in terms of leverage.

The paper is organized as follows. Section 2 introduces the Ariel Mission Candidate Sample (MCS) dataset \mathcal{T} that we will be working with. Section 3 defines several different selection methods and discusses the corresponding heuristics used in their implementation. Section 4 contains our numerical results and compares the different outcomes in selecting the mission target list \mathcal{S} . Section 5 discusses the advantages and limitations of our approach.

2. DATA

The Mission Candidate Sample for the Ariel mission was defined in Edwards & Tinetti (2022). The MCS is regularly updated and can be found on the Ariel mission GitHub page¹. For this study we used the update from August 18th 2025, which is the latest update available at the time of writing. It includes both confirmed planets and TESS planetary candidates, resulting in 2696 objects. For brevity, we will refer to the objects in that sample as “planets”, regardless of whether they have been confirmed yet. We decided to focus on planets that will necessitate no more than 20 transits to build up Tier 2 signal-to-noise ratio (SNR), which is the upper limit required for Tier-2 observations (Edwards & Tinetti 2022). This reduces the initial MCS list to 1343 planets. We also removed an odd candidate with a planet radius larger than 10 Jupiter radii, obtaining a final sample of 1342 planets. This sample is illustrated in Figure 1 as scatter plots of the required Tier-2 observational time versus each of the planet parameters in $\{p\} = \{R_p, T_p, T_s\}$. We note that our method can be applied to any other set of planetary parameters of interest, but we decided to use these three for consistency with previous studies (Edwards & Tinetti 2022; Hord et al. 2024; Cowan & Coull-Neveu 2025). The observation time of each planet transit is taken as three times the actual transit duration. While the usual guideline is to adopt 2.5 times the transit duration to account for the baseline needed before and after the transit, we use a factor of 3 to include additional margin for telescope slew and settling time. For the purposes of this paper, we consider a three year Ariel Tier-2 transit survey ($T = 3$ years).

3. METHODS

¹ https://github.com/arielmission-space/Mission_Candidate_Sample

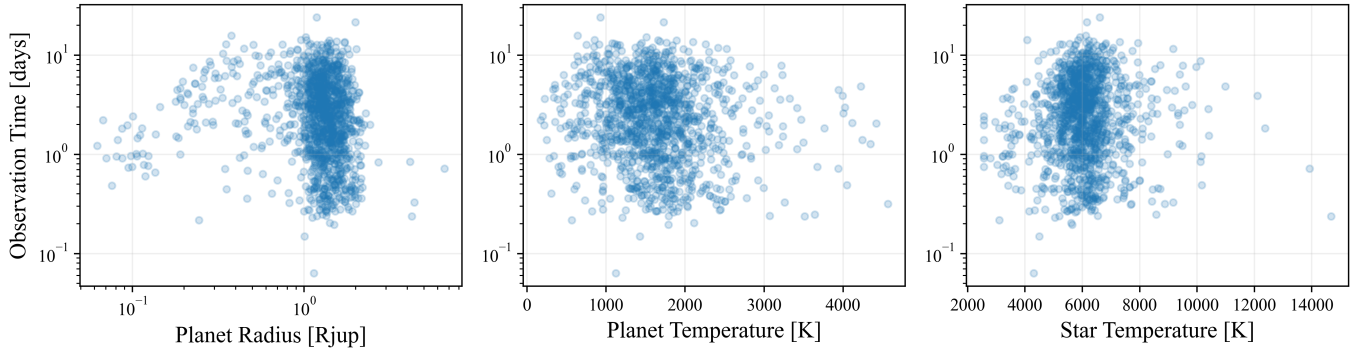


Figure 1. Total observing time required to reach an Ariel Tier 2 SNR versus the planet radius (left panel), the planet equilibrium temperature (middle panel) or the effective temperature of the star (right panel).

In this section we introduce several examples for the objective function $f(\mathcal{S})$ and in each case discuss the computational strategy for selecting the optimal subsample \mathcal{S} .

3.1. Sample size (time greedy selection)

One simple choice is to maximize the number of observed planets:

$$f_t(\mathcal{S}) = |\mathcal{S}| = N, \quad (2)$$

where the vertical bars denote the cardinality of the set \mathcal{S} , i.e., the number of elements N in \mathcal{S} . This is a very conservative choice, which makes sense in cases where it is not immediately obvious (or there is no consensus agreement) what are the important parameters $\{p\}$ to diversify. The overall time budget constraint (1) implies that this choice of f prioritizes the planets that need the least observation time, hence the index “ t ” in (2). In this scenario, the numerical procedure of selecting the optimal \mathcal{S} is very simple: we rank-order all planets in our dataset by their observation time t_i and apply a **time greedy** selection, starting from the easiest to observe planet, and continuing until the total available observation time T is exhausted. The resulting selection is identical to the Single Class method described in Cowan & Coull-Neveu (2025).

3.2. Sample variety (variance greedy selection)

At the other extreme, one could prioritize diversity of the sample along some chosen parameter p , and thus define the objective function to be the corresponding variance:

$$f_v(\mathcal{S}) = \frac{1}{N} \sum_{i \in \mathcal{S}} (p_i - \bar{p}_{\mathcal{S}})^2 \equiv \frac{1}{N} \sum_{i \in \mathcal{S}} v_i, \quad (3)$$

where

$$\bar{p}_{\mathcal{S}} \equiv \frac{1}{N} \sum_{i \in \mathcal{S}} p_i \quad (4)$$

is the average value of the parameter p within the selected subsample \mathcal{S} and v_i denotes the contribution of planet i to the sum in (3), hence the subscript “ v ”. As before, $N = |\mathcal{S}|$ denotes the number of elements in \mathcal{S} .

To select the subsample which maximizes (3), we can follow a similar greedy selection procedure as in the previous subsection, ordering the planets by their respective v_i . However, there is an

important subtlety: the mean $\bar{p}_{\mathcal{S}}$ is not known a priori, and so we cannot compute the squared deviations $v_i = (p_i - \bar{p}_{\mathcal{S}})^2$ exactly. At the same time, for a large enough subsample \mathcal{S} , we can reasonably assume that the sample mean is very close to the population mean

$$\bar{p}_{\mathcal{T}} \equiv \frac{1}{|\mathcal{T}|} \sum_{i \in \mathcal{T}} p_i, \quad (5)$$

which is known to us in advance. We can thus make the approximation $\bar{p}_{\mathcal{S}} \approx \bar{p}_{\mathcal{T}}$ and rank-order the planets by the squared deviations $v_i = (p_i - \bar{p}_{\mathcal{T}})^2$ instead, starting the selection from the largest v_i and proceeding until the total available observation time T is exhausted. In what follows, we shall refer to the resulting selection as “variance greedy”.

3.3. Sample leverage

A major science goal of Ariel is to quantify population-level trends in atmospheric properties. The simplest trends are linear: $y = mp + b$, where y represents a derived planetary property measured with Ariel, while p is our previously discussed planetary parameter along an axis of diversity (Thorngren et al. 2016; Welbanks et al. 2019; Swain et al. 2024). The constants m and b need to be extracted from a fit to the data collected from the sample \mathcal{S} of observational targets. Therefore, the choice of \mathcal{S} impacts the subsequent precision with which m and b could be determined. Cowan & Coull-Neveu (2025) pointed out that the uncertainty σ_m on the fitted slope m is inversely proportional to the leverage L and therefore, L is a sensible choice for the objective function f . In order to avoid dealing with square roots, in this work we find it more convenient to introduce the leverage squared:

$$f_L(\mathcal{S}) = L^2(\mathcal{S}) = N \cdot \mathbf{Var}(p) = \sum_{i \in \mathcal{S}} (p_i - \bar{p}_{\mathcal{S}})^2 = \sum_{i \in \mathcal{S}} v_i, \quad (6)$$

where $\bar{p}_{\mathcal{S}}$ and v_i are the same quantities appearing in eq. (3). The objective function f_L strikes a balance between sample size (through the N factor) and diversity (through the $\mathbf{Var}(p)$ factor).

The mathematical problem of choosing the optimal subsample \mathcal{S} which maximizes the objective function (6) is rather nontrivial. Cowan & Coull-Neveu (2025) proposed a couple of heuristic methods (Sections 3.3.1-3.3.2) which for reference we include in our numerical analysis in the next section. In this paper, we consider three additional methods (Sections 3.3.3-3.3.5), among which the “leverage greedy” approach of Section 3.3.4 is designed to provide the best possible answer. For completeness, we shall also illustrate what happens if the selection is done totally at random, ignoring any objective function f (Section 3.3.6).

3.3.1. Regular classes

To broaden the variety of studied exoplanets, they are typically divided into specific groups, such as hot Jupiters, warm sub-Neptunes, lava planets, etc., and then the target selection is done by picking the easiest to observe target from each group, alternating between the classes until the observation budget is full (Edwards & Tinetti 2022; Hord et al. 2024). This strategy relies on an appropriate definition of the planetary classes. To define the planet groups, Cowan & Coull-Neveu (2025) used the parameter axes of diversity, anticipating that this approach would result in a selection with high leverage. They considered two possibilities: regular binning and quantile binning.

With regular binning, the relevant range along each axis of diversity is divided into a fixed number of equal-length subintervals. Cowan & Coull-Neveu (2025) considered up to 20 subintervals and

showed that splitting into so many is typically unnecessary, since the highest-leverage was observed in selections done with just a handful of classes. For concreteness, in our numerical experiments in the next section, we shall adopt the default of 3 classes used in Cowan & Coull-Neveu (2025).

3.3.2. Quantile classes

Since planet populations tend to be not uniformly spread along the axes of diversity, regular binning runs into the problem of insufficient counts in certain sparsely populated bins. As a result, the selection algorithm may reach a point where there are no planets left in a class to choose from. To avoid this problem, Cowan & Coull-Neveu (2025) also considered using quantile bins along the axes of diversity, so that each class contains the same number of planets. As before, the algorithm selects the cheapest (in terms of required observation time) planet, alternating between the classes until the total budget T is exhausted. Following Cowan & Coull-Neveu (2025) we shall illustrate this scenario also with 3 quantile bins per axis.

3.3.3. K -means clustering

An alternative method of separating planets into classes is to use unsupervised machine learning clustering techniques. For example, K -means clustering finds a predefined number of K clusters of planets in the data (Hayes et al. 2020; Matchev et al. 2022). Note, however, that the number of planets that end up in a given cluster is unconstrained, and is determined by the clustering algorithm. The selection algorithm then again cycles between the clusters, selecting the cheapest remaining one in each cluster, until the budget is exhausted. This approach automatically adapts to a potentially uneven distribution of planets, since the planets within each cluster have similar properties, while planets belonging to different clusters generally have different properties. For a fair comparison with the class-based methods from Sections 3.3.1 and 3.3.2, we shall use three clusters per axis.

3.3.4. Leverage greedy selection

Here we introduce our fiducial greedy algorithm. For submodular maximization of the objective function f_L with a knapsack constraint (1), this algorithm works as follows. Let the current selection be \mathcal{S}_0 . For each of the remaining planets $e_i \in \mathcal{T}$ whose selection would not cause a violation of the time budget, i.e., for which the following inequality holds

$$t_i + \sum_{k \in \mathcal{S}_0} t_k \leq T, \quad (7)$$

compute the marginal gain per unit cost

$$\frac{\Delta f_L(e_i)}{\Delta t} = \frac{f_L(\mathcal{S}_0 \cup e_i) - f_L(\mathcal{S}_0)}{t(\mathcal{S}_0 \cup e_i) - t(\mathcal{S}_0)} = \frac{f_L(\mathcal{S}_0 \cup e_i) - f_L(\mathcal{S}_0)}{t_i} \quad (8)$$

and proceed iteratively with a greedy selection. As the name suggests, the ratio (8) quantifies the benefit (in terms of the objective function f_L) from adding a single element e_i with a cost t_i to the existing selection \mathcal{S}_0 , keeping in mind the budgetary constraint. Using the definition (6), we can express the marginal gain simply as

$$\frac{\Delta f_L}{\Delta t} = \frac{v_i}{t_i} = \frac{(p_i - \bar{p}_{\mathcal{S}_0})^2}{t_i}, \quad (9)$$

where in analogy to (4), $\bar{p}_{\mathcal{S}_0}$ is the average value of the parameter p over the set \mathcal{S}_0 . Since the values of p_i and t_i for each planet are known in advance, and the average $\bar{p}_{\mathcal{S}_0}$ can be updated at the start of each iteration, Eq. (9) provides a simple ranking criterion for our “leverage-greedy” method, which balances both variance and number of planets as it prioritizes planets with the highest leverage score (9).

Note that in cases where the size of the optimal subsample \mathcal{S} is large enough to justify the approximation $\bar{p}_{\mathcal{S}_0} \approx \bar{p}_{\mathcal{T}}$ at all times, we can use an alternative criterion in terms of the population average $\bar{p}_{\mathcal{T}}$

$$\frac{\Delta f_L}{\Delta t} = \frac{v_i}{t_i} = \frac{(p_i - \bar{p}_{\mathcal{T}})^2}{t_i}, \quad (10)$$

which leads to a further simplification since it allows the marginal gains (10) to be precomputed once and for all.

In conclusion of this subsection, let us motivate the marginal gain ratio as the right variable to use with the following simple gedanken experiment. As a starting point, consider a randomly selected subsample \mathcal{S}_0 which saturates the time budget constraint in the sense that

$$\sum_{k \in \mathcal{S}_0} t_k \simeq T, \quad (11)$$

so that adding any other additional planet would violate the inequality (7). Since this \mathcal{S}_0 was chosen at random, it is far from optimal, and we can improve the leverage by adding a judiciously chosen planet i from the remaining set in \mathcal{T} . However, in order to stay under budget, we have to simultaneously eliminate one of the existing planets, say j , which is already in \mathcal{S}_0 . As a result of this swap between planets i and j , the objective function (6) changes by

$$\Delta f_L = v_i - v_j. \quad (12)$$

However, now we need to take into account the relative costs t_i and t_j . If the removed planet had a larger cost, this allows us in effect to add not just one, but t_j/t_i copies of our planet i (assuming an infinite reservoir \mathcal{T}). This will keep the budget the same, and lead to a change in the objective function

$$\Delta f_L = \frac{t_j}{t_i} v_i - v_j = t_j \left(\frac{v_i}{t_i} - \frac{v_j}{t_j} \right), \quad (13)$$

which makes it clear that the benefit depends only on the ratio v/t , in agreement with eqs. (8-10).

3.3.5. Simulated annealing

Simulated annealing is a flexible search method designed to explore the space of possible subsamples beyond purely greedy choices described in (9) or (10). Starting from an initial feasible subset, we generate trial moves by randomly adding, removing, or swapping planets, with the resulting subset remaining within the total observing time budget. Each proposed move is evaluated based on its effect on the leverage objective function f_L . In order to avoid getting stuck in local maxima, the annealing algorithm is allowed in principle to accept worse solutions within some tolerance. The algorithm keeps track of a variable (the temperature Θ) that controls how likely it is for worse changes to be

accepted. If the proposed change improves the leverage, it is always accepted. If it does not improve the leverage, it is accepted with probability:

$$P = \exp\left(\frac{L(\text{new}) - L(\text{current})}{\Theta}\right),$$

where L is the leverage and Θ is the temperature. Over the course of the optimization the temperature decreases, making the algorithm more conservative. Unlike the leverage-greedy algorithm, simulated annealing does not rely on marginal gains per unit cost and therefore provides an independent consistency check on the quality of greedy solutions, at the expense of increased computational cost.

3.3.6. Random selection

To understand how the heuristic methods above compare to random selection, we also sample random subsets uniformly from all possible subsets that (almost) saturate the time constraint. They provide a useful baseline for Figure 4 below and represent the result from blind selection, without applying any optimization.

3.4. Multiple axes of diversity

While our previous discussion was focused on a single parameter of interest, it can be easily generalized to multiple parameters of diversity. To be specific, let us represent the set of parameters of interest $\{p^{(1)}, p^{(2)}, \dots, p^{(N_p)}\}$ with the vector \vec{p} . In analogy to (5), let us define the population mean

$$\langle \vec{p} \rangle_{\mathcal{T}} \equiv \frac{1}{|\mathcal{T}|} \sum_{i \in \mathcal{T}} \vec{p}_i. \quad (14)$$

Then all of our previous discussion still holds, by replacing p with \vec{p} and \bar{p} with $\langle \vec{p} \rangle_{\mathcal{T}}$, e.g.

$$f_L(\mathcal{S}) = N \cdot \mathbf{Var}(\vec{p}) = \sum_{i \in \mathcal{S}} (\vec{p}_i - \langle \vec{p} \rangle_{\mathcal{S}})^2 \simeq \sum_{i \in \mathcal{S}} (\vec{p}_i - \langle \vec{p} \rangle_{\mathcal{T}})^2. \quad (15)$$

Note that when we write out (15) explicitly:

$$f_L(\mathcal{S}) = \sum_{i \in \mathcal{S}} (\vec{p}_i - \langle \vec{p} \rangle_{\mathcal{T}})^2 = \sum_{k=1}^{N_p} \sum_{i \in \mathcal{S}} \left(p_i^{(k)} - \langle p^{(k)} \rangle_{\mathcal{T}} \right)^2 \quad (16)$$

we see that the sum involves terms with different physical units, which may therefore have very different magnitudes. In such cases, the optimization algorithm will focus on the parameters with the largest numerical values (in their respective physical units) and will largely ignore the others. To prevent this, it is common in machine learning to “standardize” each parameter $p^{(k)}$ by centering around its population mean $\langle p^{(k)} \rangle_{\mathcal{T}}$ and rescaling by its standard deviation $\sigma_{\mathcal{T}}^{(k)}$:

$$p_i^{(k)} \rightarrow \hat{p}_i^{(k)} \equiv \frac{p_i^{(k)} - \langle p^{(k)} \rangle_{\mathcal{T}}}{\sigma_{\mathcal{T}}^{(k)}}. \quad (17)$$

In what follows, in multi-parameter cases we shall use these standardized variables $\hat{p}^{(k)}$.

Method	Planets selected	Leverage score	% of budget used
1 parameter: Equilibrium temperature only			
Time greedy	765	29.30	99.76%
Variance greedy	326	32.99	99.94%
Leverage greedy	530	34.08	100.00%
Regular classes	753	29.13	99.87%
Quantile classes	761	28.38	99.84%
K-means clustering	678	32.30	99.92%
Simulated annealing	698	33.33	99.94%
2 parameters: Planet radius + Equilibrium temperature			
Time greedy	765	42.03	99.76%
Variance greedy	344	45.81	99.80%
Leverage greedy	551	47.63	99.99%
Regular classes	678	41.23	99.99%
Quantile classes	613	35.31	99.49%
K-means clustering	678	44.13	99.92%
Simulated annealing	695	45.80	99.93%
3 parameters: Planet radius + Equilibrium temperature + Stellar Temperature			
Time greedy	765	52.06	99.76%
Variance greedy	349	56.08	99.41%
Leverage greedy	568	58.52	99.86%
Regular classes	650	53.80	99.85%
Quantile classes	502	34.31	99.39%
K-means clustering	605	56.14	99.59%
Simulated annealing	696	56.70	99.93%

Table 1. Comparison of selection heuristics across 1D, 2D, and 3D parameter spaces. We quote the number of planets selected, the leverage score, and the percentage of the time budget that is utilized, i.e. $\frac{1}{T} \sum_{k \in \mathcal{S}} t_k$. For simplicity, here we report the leverage and not the leverage squared.

4. RESULTS

The numerical results from our experiments are summarized in Table 1, while Figures 2-4 illustrate the planetary target selections resulting from the different methods discussed in Section 3. We perform three different exercises: a one-parameter exercise, where the diversity parameter is chosen to be the planet equilibrium temperature (top section of Table 1); a two-parameter exercise, where the parameters of interest are the planet radius and equilibrium temperature (middle section of Table 1); and a three-parameter exercise, where the parameters of interest are the planet radius, the planet equilibrium temperature and the effective temperature of the star (bottom section of Table 1).

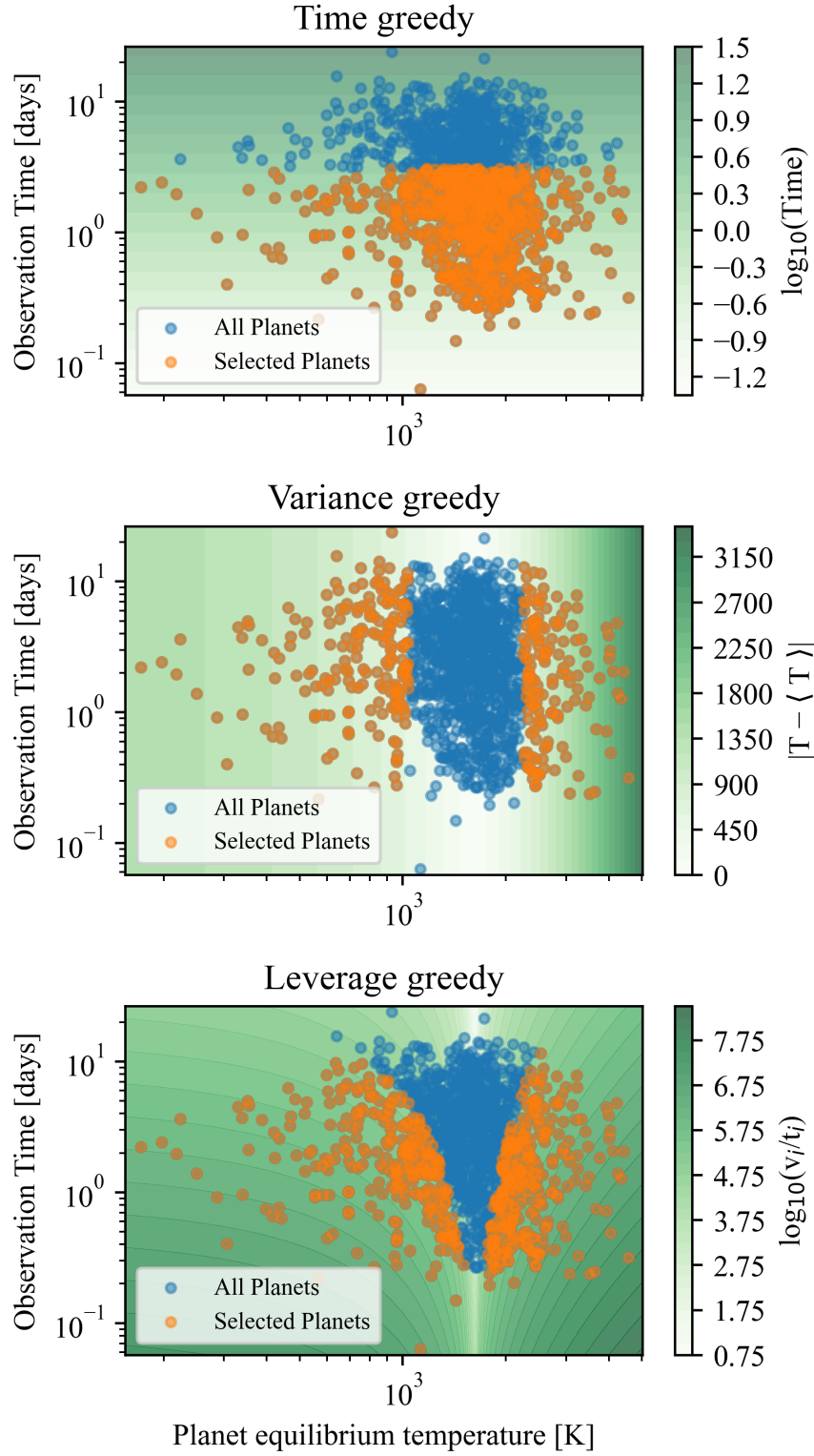


Figure 2. One-parameter exercise. Subpopulation of selected planets (in orange) using different selection objectives: sample size (eq. (2), top panel), sample variety (eq. (3), middle panel) and sample leverage (eq. (6), bottom panel). The color-coding indicated on the colorbar represents the contribution of an individual planet to the total time budget T (top panel) or to the objective function (middle and lower panels).

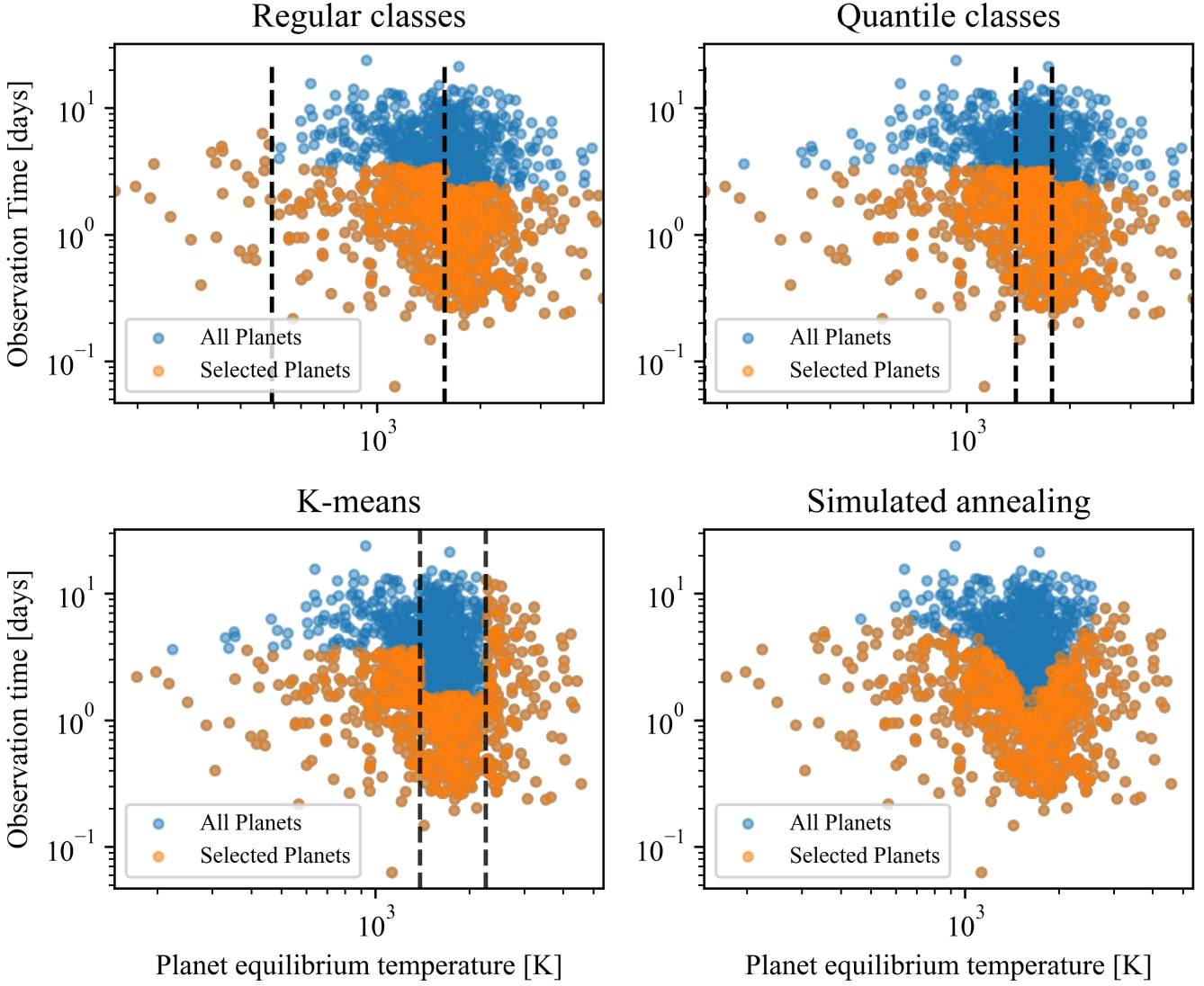


Figure 3. One-parameter exercise. Subpopulations of selected planets (in orange) for the leverage objective function (6), using alternative heuristics for maximizing the objective function: regular classes (Section 3.3.1, top left panel), quantile classes (Section 3.3.2, top right panel), K-means clustering (Section 3.3.3, bottom left panel) and simulated annealing (Section 3.3.5, bottom right panel). The selection using the leverage-greedy algorithm of Section 3.3.4 was already shown in the bottom panel of Figure 2.

In each exercise, we consider the three different objective functions defined in eqs. (2), (3) and (6), and report the respective results on the first three lines of each section in Table 1. When the objective is to maximize the sample leverage, we discuss five different heuristics for performing the planet selection (see Sections 3.3.1-3.3.5). The corresponding results are quoted in the last five rows in each section of the table. We observe that in each exercise, the leverage-greedy algorithm outperforms the other four heuristics in terms of maximizing the leverage. This is why for the one-parameter exercise depicted in Figure 2 we only show the result from the leverage-greedy selection of Section 3.3.4. For completeness, the results for the remaining four heuristics are collected in Figure 3.

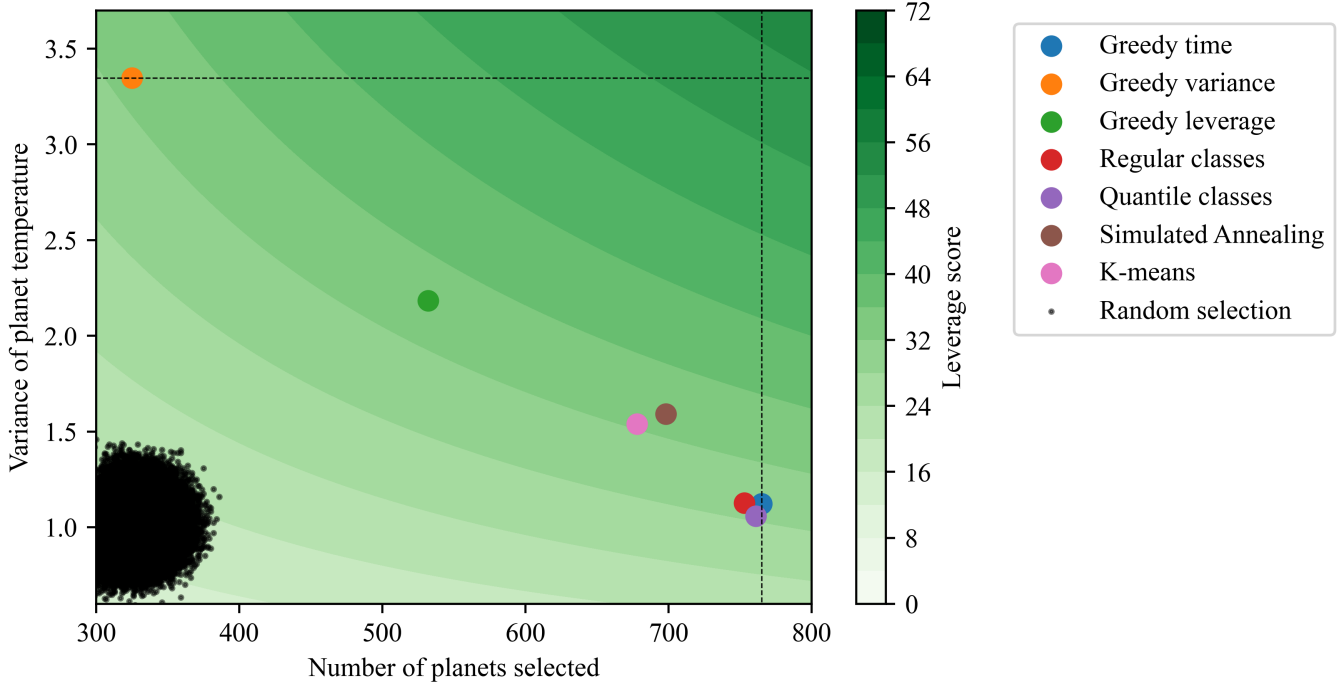


Figure 4. A summary plot of the performance of all the different selection methods discussed in the paper for the one-parameter exercise. Colored circles correspond to the seven selection strategies shown in Table 1, while black dots represent randomly chosen subsets. The background is shaded according to the leverage of the selected subset.

Each panel in Figures 2 and 3 is showing the entire sample of 1342 planets (blue points), as a scatter plot in the plane of observation time versus planet equilibrium temperature. The selected planets are overplotted in orange. The green shading in Figure 2 indicates the contribution of an individual planet to the total time budget T (top panel) or to the objective function (middle and lower panels). This color-coding helps understand how greedy algorithms work — they start the selection from the most beneficial region and gradually progress through the adjacent green bands until the time budget is exhausted. For example, in the top panel of Figure 2, the selection proceeds from bottom to top, starting with the planets easiest to observe. Similarly, in the middle panel of Figure 2, the selection starts from the outliers on the left and right sides (having the largest variance $v_i = (T_i - \langle T \rangle)^2$) and progresses towards the middle. In the bottom panel of Figure 2, the selection starts from the planets with the largest variance per unit time, v_i/t_i , (dark green) and proceeds towards the central region.

Figure 2 demonstrates that different objective functions result in different selected samples. As seen in Table 1, the time-greedy method by design always maximizes the number of observed planets, although many of them share very similar characteristics. In particular, planets which have large variance but require a lot of observational time, are missed. On the other hand, the variance greedy method selects all outliers, regardless of their observational cost, leading to a rather small (typically by a factor of 2) target sample. In addition, many of the typical planets in the population are completely missed because the core of the distribution is not sampled. The leverage greedy method is trading some of the high-variance, high-cost planets for many more lower-variance, lower-cost planets, in order to strike the right balance between sample size and sample diversity. The resulting selection

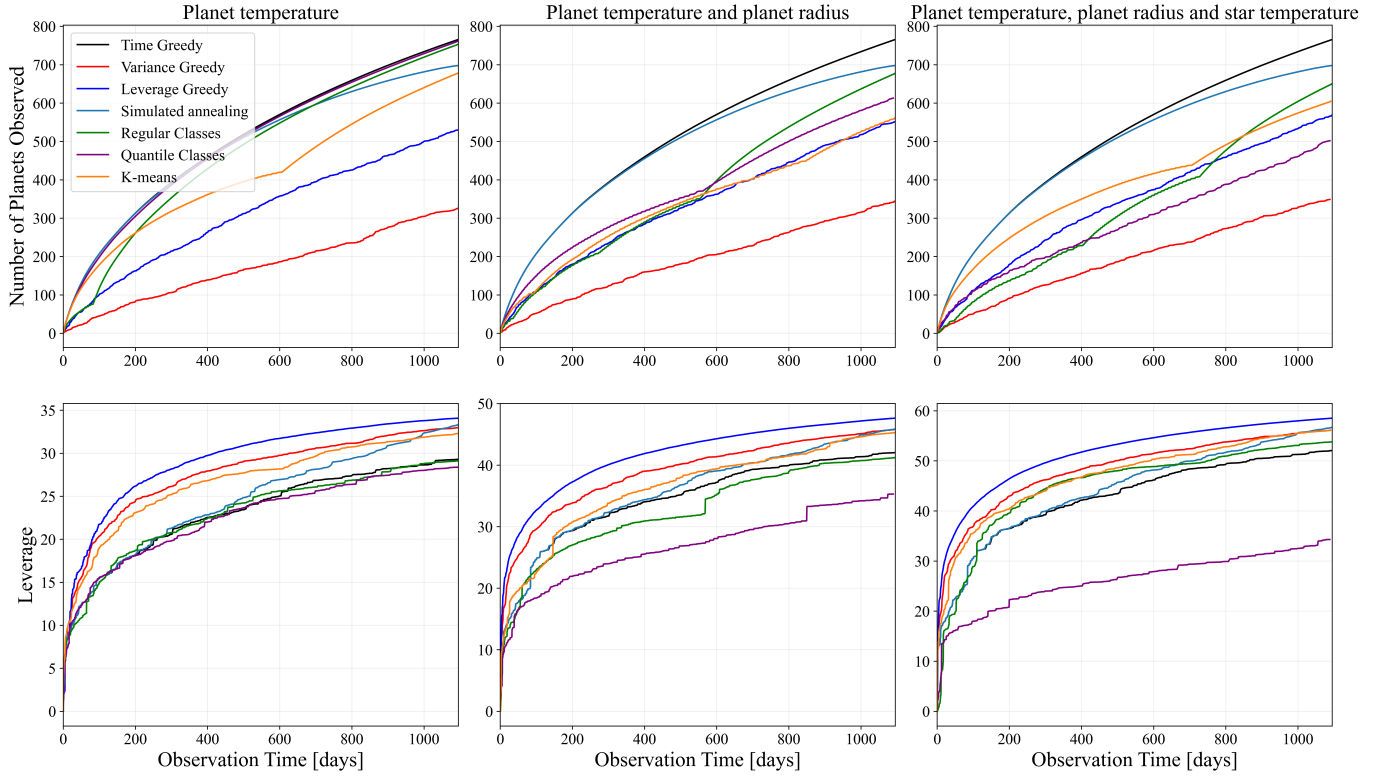


Figure 5. Comparison of cumulative curves for each of the seven selection strategies discussed in the paper. The top row is showing the number of planets selected as a function of observation time in days. The bottom row is similarly showing the sample leverage as a function of observation time. The left (middle, right) columns represent the results for the one- (two-, three-) parameter exercise, respectively.

more evenly samples the original population, although the “typical” population is still somewhat underrepresented.

Figure 4 is a summary plot of the performance of all the different selection methods discussed in the paper for the one-parameter exercise. It illustrates the achieved leverage (color bar) of a given selection method on a scatter plot of sample variance versus sample size. Each point represents a possible sample selection and the green color contours outline samples of constant leverage. Each of the discussed sample selection strategies is shown with a colored circle as indicated in the legend. It is clear that the time greedy selection maximizes the number of selected planets given the mission time constraint, while the variance greedy selection represents the other end of the spectrum, maximizing the variance of the selected sample. Both of these methods are outperformed in terms of leverage by the leverage greedy selection. This figure demonstrates well that both the “regular-classes” and “quantile-classes” selections perform very similar to the time-greedy method in terms of leverage and number of selected planets in agreement with the conclusions in Cowan & Coull-Neveu (2025). It also makes clear that the simulated-annealing method gives very competitive results in terms of leverage, while it also allows for a large sample size. K-means clustering presents a viable alternative worth investigating, particularly if the dataset contains well-defined, distinct subgroups.

As a baseline for comparison, we also sample random subsets uniformly from all possible subsets of the original planet population which satisfy the time constraint (see Section 3.3.6). The random subsets (shown as black dots) tend to cluster in the bottom-left region of the plot, indicating the

worst case: a low number of planets and a low variance. We can see that all optimization methods present a substantial improvement compared to the random subsets, which is reassuring. In other words, it pays off to have a global selection strategy, which motivates a community discussion about the science priorities and the mission constraints, having in mind the entire planet population rather than individually selected planets.

Figure 5 presents cumulative curves similar to Figure 3 in Cowan & Coull-Neveu (2025) of each selection method as a function of the observing time. The top row shows the cumulative number of targets as a function of the observing budget for 1-parameter, 2-parameter, and 3-parameter experiments. As expected, the time greedy approach (black line) is maximizing the number of observed planets. The bottom row compares the cumulative leverage. The leverage greedy and simulated annealing strategies consistently achieve a higher leverage value for a given observing time, indicating a better trade-off between diversity and efficiency. Class-based and clustering methods occupy an intermediate regime, offering structured coverage of the parameter space but lower total leverage.

5. SUMMARY AND CONCLUSIONS

In this work we compared several approaches for selecting exoplanet targets under an observation time constraint. We introduced three different selection criteria (sample size, sample variance, and sample leverage) and quantified them in terms of suitable objective functions, allowing for the application of modern optimization algorithms. We considered five different heuristics for maximizing the sample leverage (leverage greedy, simulated annealing, K-means clustering, regular classes and quantile classes). The outcomes from the different selection methods were illustrated with three exercises (each with one, two, or three axes of diversity, respectively) and the results were collected in Table 1 and Figures 2-5.

Each selection criterion highlights a different compromise between the number of planets selected, their diversity and the total observation time required. The time greedy selection maximizes the number of planets but not the diversity. The variance greedy selection maximizes diversity, but that comes at a cost: it overemphasizes rare cases, undersamples the most typical planets, and in general, sacrifices the number of planets which can be observed. The leverage greedy selection appears to be a good compromise for balancing sample diversity and sample size.

Table 1 and Figure 4 demonstrate that among the five heuristics for optimizing the leverage, the leverage greedy selection performs best. Simulated annealing is always second-best and provides an excellent alternative, with a significantly increased sample size for a very modest reduction in leverage. In contrast to the leverage greedy selection, the selection with simulated annealing is much more representative of the original population, and covers both rare and typical planets (see lower right panel in Figure 3). Binning or clustering methods can give structured coverage of the parameter space.

We note that the use of standardized variables (17) allows us to easily generalize the discussion to several axes of diversity, as shown in the middle and right columns in Figure 5. Furthermore, it helps us understand the scaling of the sample leverage with a different number of axes of diversity (i.e., parameters of interest N_p). Note that the number of terms in the sum (16) representing the leverage *squared* scales with N_p , therefore the leverage itself scales with $\sqrt{N_p}$. This can be easily verified by the results in Table 1: the maximal leverage obtained in the one-parameter exercise was ~ 34 , so for the two-parameter exercise we should expect $\sim 34 \times \sqrt{2} \sim 48$, and that is precisely what is seen

in the middle section of Table 1. Similarly, for the three-parameter exercise we would expect the maximal leverage to be $\sim 34 \times \sqrt{3} \sim 58.9$, again in agreement with the lower section of Table 1.

In all examples considered in this paper, we always used a single selection criterion (objective function) throughout the selection process. An alternative could be to combine multiple strategies. For example, we could first use leverage to secure diversity in a small subset of targets, while using another criterion (or a list of specific targets of interest) for the remainder of the selection. That would ensure that unusual planets are represented, while also having enough typical planets or planets of interest selected.

As discussed in Cowan & Coull-Neveu (2025), the leverage is directly related to the uncertainty on the slope of linear trends. In future work, we plan to apply our approach to the mass-metallicity relation for exoplanets, as it is one of the most fundamental population-level trends noted in the literature (Thorngren et al. 2016; Welbanks et al. 2019; Sun et al. 2024; Swain et al. 2024). This will provide a physically motivated test case linking optimization of target selection to potential scientific results of the Ariel mission. We also plan to incorporate ephemerides and scheduling constraints, as the periodic observability of exoplanets critically affects the selection of targets. Taking into account these factors will bring the optimization closer to real mission planning.

ACKNOWLEDGMENTS

The work of EP, AR and KTM is supported in part by the Shelby Endowment for Distinguished Faculty at the University of Alabama. N.B.C. acknowledges support from an NSERC Discovery Grant and a Tier 2 Canada Research Chair, and thanks the Trottier Space Institute and l’Institut de recherche sur les exoplanètes for their financial support and dynamic intellectual environment. The authors thank Ben Coull-Neveu for sharing his codes from the previous related study in Cowan & Coull-Neveu (2025).

REFERENCES

Barclay, T., Quintana, E. V., Colón, K., et al. 2025, arXiv e-prints, arXiv:2502.09730, doi: [10.48550/arXiv.2502.09730](https://doi.org/10.48550/arXiv.2502.09730)

Batalha, N. E., Wolfgang, A., Teske, J., et al. 2023, AJ, 165, 14, doi: [10.3847/1538-3881/ac9f45](https://doi.org/10.3847/1538-3881/ac9f45)

Burt, J. A., Zellem, R. T., Ciardi, D. R., et al. 2025, AJ, 170, 216, doi: [10.3847/1538-3881/adf5ba](https://doi.org/10.3847/1538-3881/adf5ba)

Cowan, N. B., & Coull-Neveu, B. 2025, Maximizing Ariel’s Survey Leverage for Population-Level Studies of Exoplanets. <https://arxiv.org/abs/2506.06429>

Edwards, B., & Tinetti, G. 2022, The Astronomical Journal, 164, 15, doi: [10.3847/1538-3881/ac6bf9](https://doi.org/10.3847/1538-3881/ac6bf9)

Edwards, B., Rice, M., Zingales, T., et al. 2019, Experimental Astronomy, 47, 29, doi: [10.1007/s10686-018-9611-4](https://doi.org/10.1007/s10686-018-9611-4)

Gardner, J. P., Mather, J. C., Clampin, M., et al. 2006, Space Science Reviews, 123, 485–606, doi: [10.1007/s11214-006-8315-7](https://doi.org/10.1007/s11214-006-8315-7)

Gardner, J. P., Mather, J. C., Abbott, R., et al. 2023, Publications of the Astronomical Society of the Pacific, 135, 068001, doi: [10.1088/1538-3873/acd1b5](https://doi.org/10.1088/1538-3873/acd1b5)

Hayes, J. J. C., Kerins, E., Awiphan, S., et al. 2020, MNRAS, 494, 4492, doi: [10.1093/mnras/staa978](https://doi.org/10.1093/mnras/staa978)

Hord, B. J., Kempton, E. M.-R., Evans-Soma, T. M., et al. 2024, AJ, 167, 233, doi: [10.3847/1538-3881/ad3068](https://doi.org/10.3847/1538-3881/ad3068)

Matchev, K. T., Matcheva, K., & Roman, A. 2022, The Planetary Sciences Journal, 3, 205, doi: [10.3847/PSJ/ac880b](https://doi.org/10.3847/PSJ/ac880b)

Rauer, H., Aerts, C., Cabrera, J., et al. 2025, Experimental Astronomy, 59, 26, doi: [10.1007/s10686-025-09985-9](https://doi.org/10.1007/s10686-025-09985-9)

Stotisbury, I., Edwards, B., Lavigne, J.-F., et al. 2022, in Space Telescopes and Instrumentation 2022: Optical, Infrared, and Millimeter Wave, ed. L. E. Coyle, M. D. Perrin, & S. Matsuura (SPIE), 235, doi: [10.1117/12.2641373](https://doi.org/10.1117/12.2641373)

Sun, Q., Wang, S. X., Welbanks, L., Teske, J., & Buchner, J. 2024, A revisit of the Mass-Metallicity Trends in Transiting Exoplanets. <https://arxiv.org/abs/2402.08292>

Swain, M. R., Hasegawa, Y., Thorngren, D. P., & Roudier, G. M. 2024, SSRv, 220, 61, doi: [10.1007/s11214-024-01098-7](https://doi.org/10.1007/s11214-024-01098-7)

Thorngren, D. P., Fortney, J. J., Murray-Clay, R. A., & Lopez, E. D. 2016, ApJ, 831, 64, doi: [10.3847/0004-637X/831/1/64](https://doi.org/10.3847/0004-637X/831/1/64)

Tinetti, G., Drossart, P., Eccleston, P., et al. 2018, Experimental Astronomy, 46, 135, doi: [10.1007/s10686-018-9598-x](https://doi.org/10.1007/s10686-018-9598-x)

Tinetti, G., Eccleston, P., Haswell, C., et al. 2021, Ariel: Enabling planetary science across light-years. <https://arxiv.org/abs/2104.04824>

Welbanks, L., Madhusudhan, N., Allard, N. F., et al. 2019, The Astrophysical Journal Letters, 887, L20, doi: [10.3847/2041-8213/ab5a89](https://doi.org/10.3847/2041-8213/ab5a89)

Zhang, T., Wilcock, B., Ma, S., et al. 2025, Atmospheric Characterisation with the Twinkle Space Telescope Following Advances from JWST Observations. <https://arxiv.org/abs/2508.10386>